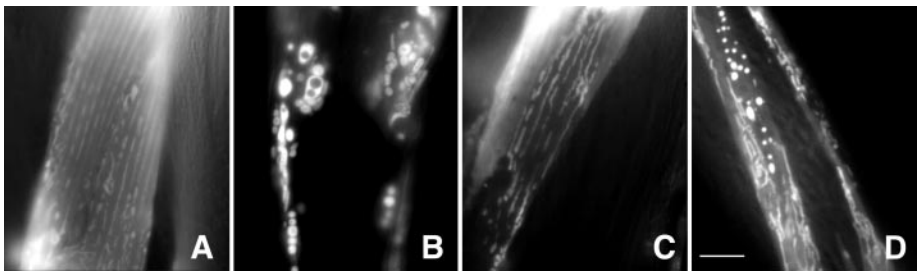

Fig. 4. GFP-labeled mitochondria are shown in the body wall muscle cells of L4 animals of the following genotypes: (**A**) wild-type *N2*, (**B**) *anc-1(e1873)*, (**C**) *unc-84(n369)*, and (**D**) cofilin *unc-60(r398)*. The severely abnormal mitochondria in *anc-1(e1873)* are not anchored. In live animals, they were seen moving throughout the muscle as the animal moved. Scale bar, 10 μm.

and spread throughout the cell as the worm moved. In contrast, mitochondria in *anc-1(e1873)* animals were spherically shaped, often clustered together, and were pushed around within the cytoplasm as the animal moved (Fig. 4B). Mitochondria were not shaped or positioned properly in an *unc-60(r398)* mutant background (Fig. 4D). A partial loss-of-function allele in the *C. elegans* cofilin homolog, *unc-60(r398)*, disrupts actin filaments in the body wall muscle of adult hermaphrodites (*23*). Therefore, actin filaments are required for proper positioning of mitochondria. The anchorage of mitochondria in *unc-84(n369)* was normal (Fig. 4C), suggesting that ANC-1 does not require UNC-84 to anchor mitochondria as it does for nuclear anchorage.

Our model (fig. S4) suggests that ANC-1 functions to anchor nuclei by tethering the nucleus to the actin cytoskeleton and predicts that the KASH domain of ANC-1 is localized to the outer nuclear envelope by UNC-84. Digitonin extraction experiments show that human Syne-2 localizes to the outer nuclear envelope (*14*). ANC-1 would then extend away from the nucleus, where its NH_2-terminus binds to the stable actin cytoskeleton. As a result, ANC-1 molecules function to directly attach the actin cytoskeleton to the nuclear envelope. Before a nucleus can migrate through the cytoplasm of the cell, the nuclear anchor must be released. The SUN domain of UNC-84 is likely to be intimately involved with this switch in nuclear behavior, because it is required for both ANC-1 and UNC-83 localization at the nuclear envelope (*21*) (Fig. 2). UNC-83 is required for normal nuclear migration but not for nuclear anchorage (*21*). It is not known whether ANC-1 and UNC-83 can interact with UNC-84 simultaneously, although both antigens are detected at the nuclear envelope of adult hypodermal cells. Overexpression of UNC-83 did not cause any obvious anchorage phenotype, eliminating a competition model.

Dystrophin and the associated dystrophin–glycoprotein complex function to connect the actin cytoskeleton to the extracellular matrix; mutations in these components lead to Duchenne or Becker muscular dystrophies (*24*). Although ANC-1 and Syne connect the actin cytoskeleton to the nuclear matrix whereas dystrophin connects actin to the extracellular matrix, there are some similarities between these two mechanisms. ANC-1 and associated proteins, including UNC-84 and lamin A/C (*12*), are likely to create a bridge across the nuclear envelope. Mutations in the gene encoding lamin A/C lead to Emery-Dreifuss muscular dystrophy (*24*), which suggests a potential link between the ANC-1 and Syne proteins and muscular dystrophy.

References and Notes

1. N. R. Morris, *J. Cell Biol.* **148**, 1097 (2000).
2. S. Reinsch, P. Gonczy, *J. Cell Sci.* **111**, 2283 (1998).
3. G. M. Guild, P. S. Connelly, M. K. Shaw, L. G. Tilney, *J. Cell Biol.* **138**, 783 (1997).
4. E. Chytilova *et al.*, *Mol. Biol. Cell* **11**, 2733 (2000).
5. J. E. Sulston, H. R. Horvitz, *Dev. Biol.* **56**, 110 (1977).
6. C. J. Malone, W. D. Fixsen, H. R. Horvitz, M. Han, *Development* **126**, 3171 (1999).
7. E. M. Hedgecock, J. N. Thomson, *Cell* **30**, 321 (1982).
8. Materials and methods are available as supporting material on *Science* Online.
9. K. L. Mosley-Bishop, Q. Li, L. Patterson, J. A. Fischer, *Curr. Biol.* **9**, 1211 (1999).
10. M. A. Welte, S. P. Gross, M. Postner, S. M. Block, E. F. Wieschaus, *Cell* **92**, 547 (1998).
11. E. D. Apel, R. M. Lewis, R. M. Grady, J. R. Sanes, *J. Biol. Chem.* **275**, 31986 (2000).
12. J. M. Mislow, M. S. Kim, D. B. Davis, E. M. McNally, *J. Cell Sci.* **115**, 61 (2002).
13. Q. Zhang *et al.*, *J. Cell Sci.* **114**, 4485 (2001).
14. Y. Y. Zhen, T. Libotte, M. Munck, A. A. Noegel, E. Korenbaum, *J. Cell Sci.* **115**, 3207 (2002).
15. Y. Rosenberg-Hasson, M. Renert-Pasca, T. Volk, *Mech. Dev.* **60**, 83 (1996).
16. T. Volk, *Development* **116**, 721 (1992).
17. Y. Yan *et al.*, *Science* **262**, 2027 (1993).
18. M. Gimona, K. Djinovic-Carugo, W. J. Kranewitter, S. J. Winder, *FEBS Lett.* **513**, 98 (2002).
19. H. R. Horvitz, J. E. Sulston, *Genetics* **96**, 435 (1980).
20. K. K. Lee *et al.*, *Mol. Biol. Cell* **13**, 892 (2002).
21. D. A. Starr *et al.*, *Development* **128**, 5039 (2001).
22. A. Fire *et al.*, *Nature* **391**, 806 (1998).
23. S. Ono, D. L. Baillie, G. M. Benian, *J. Cell Biol.* **145**, 491 (1999).
24. E. A. Burton, K. E. Davies, *Cell* **108**, 5 (2002).
25. We thank Han lab members and L. Chen for their advice; S. McCauley, G. Ackerman, and L. Chlipala for technical assistance; and the *Caenorhabditis* Genetics Center, J. Hodgkin, S. Ono, P. Mains, A. Fire, A. Coulson, and Y. Kohara for materials. Supported by NIH and Howard Hughes Medical Institute.

Supporting Online Material
www.sciencemag.org/cgi/content/full/1075119/DC1
Materials and Methods
Supporting Text
Figs. S1 to S4
References and Notes

17 June 2002; accepted 29 July 2002
Published online 8 August 2002;
10.1126/science.1075119
Include this information when citing this paper.

Neural Correlates for Perception of 3D Surface Orientation from Texture Gradient

Ken-Ichiro Tsutsui,[1]* Hideo Sakata,[1,2] Tomoka Naganuma,[1,3] Masato Taira[1]†

A goal in visual neuroscience is to reveal how the visual system reconstructs the three-dimensional (3D) representation of the world from two-dimensional retinal images. Although the importance of texture gradient cues in the process of 3D vision has been pointed out, most studies concentrate on the neural process based on binocular disparity. We report the neural correlates of depth perception from texture gradient in the cortex. In the caudal part of the lateral bank of intraparietal sulcus, many neurons were selective to 3D surface orientation defined by texture gradient, and their response was invariant over different types of texture pattern. Most of these neurons were also sensitive to a disparity gradient, suggesting that they integrate texture and disparity gradient signals to construct a generalized representation of 3D surface orientation.

The real world is three-dimensional (3D), but when projected to the retina it is reduced to a two-dimensional (2D) image. Nevertheless, what we see and what we perceive is all 3D. Therefore, the brain must be reconstructing the 3D representation of the real world from the 2D images on the retinae. Among many kinds of depth cues, binocular disparity has been suggested to be critical in many psychophysical studies (*1–3*). Neurons in striate (*4–7*) and extrastriate (*6–10*) visual areas are sensitive to binocular disparity signals. Recently, neurons that code 3D features of a visual surface by higher-order processing of

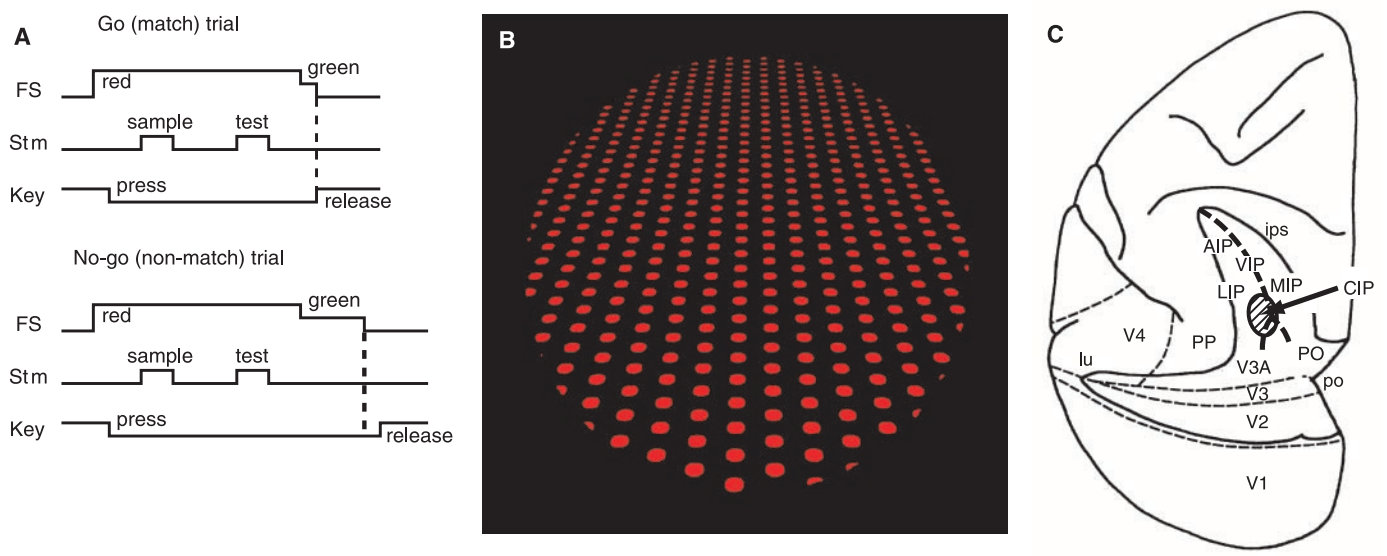

Fig. 1. (**A**) Time course of delayed match-to-sample task. To obtain a reward, monkeys had to discriminate the orientation of the sample and test stimuli and make a go or no-go response depending on whether the surface orientations of the sample and test stimuli were the same or different. Duration of stimulus presentation was about 1 s, and that of delay between sample and test stimulus presentations was about 2 s. When the test stimulus matched the sample, monkeys had to make a go response; when the test stimulus did not match the sample, they had to make a no-go response. FS = fixation spot. (**B**) Texture pattern with dot elements (dot-TP). Surface orientation of backward inclination (270° tilt) is defined by texture gradient of dot elements. By rotating the figure counterclockwise around the *z* axis, the surface orientation varies as right side nearer (0° tilt), forward (90° tilt), and left side nearer (180° tilt). Dot-TP had texture spacing cues and texture element size and shape cues for 3D orientation. Line-TP had perspective cues as well as texture spacing cues. (**C**) Schematic indicating the location of CIP. The intraparietal sulcus (ips), lunate sulcus (lu), and parietooccipital sulcus (po) are unfolded. CIP is located between areas LIP and V3A.

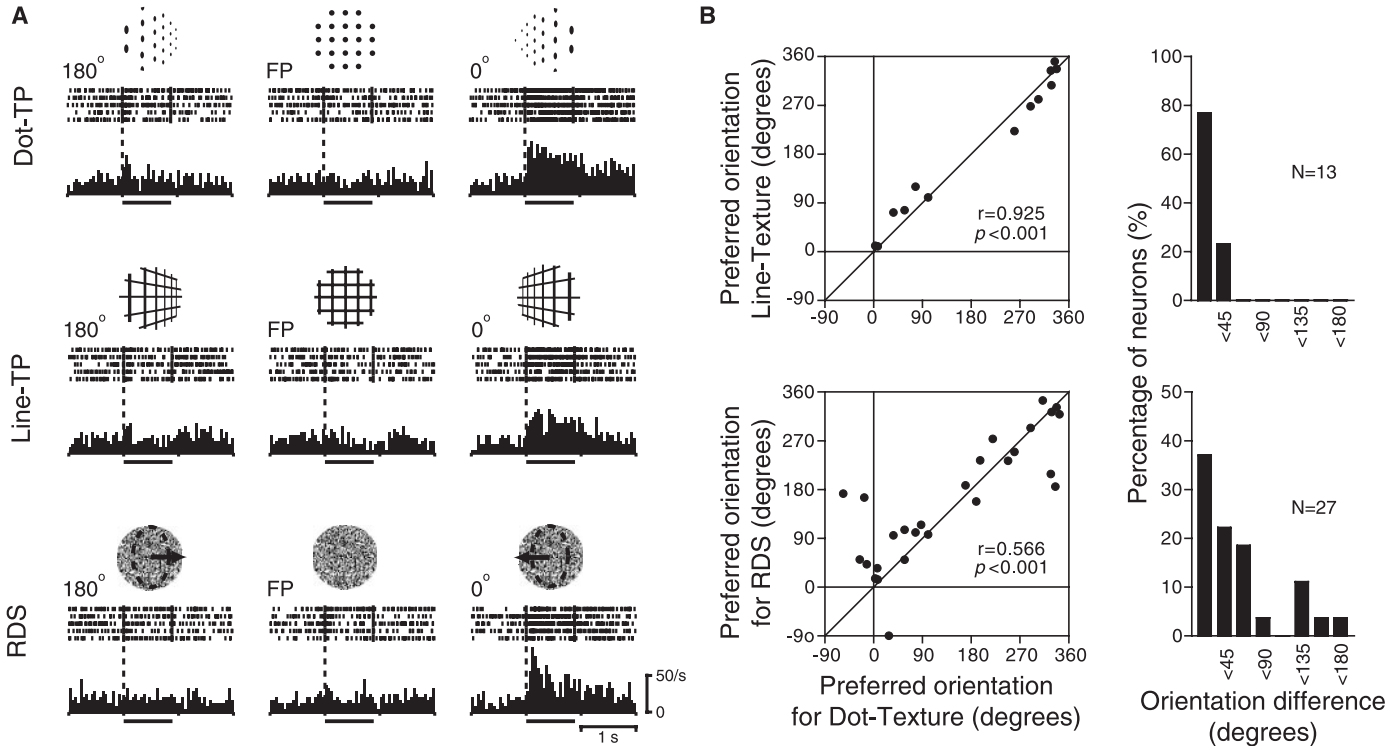

Fig. 2. (**A**) Responses of a texture gradient–sensitive neuron (*22*) to dot-TP (top row), line-TP (middle row), and RDS (bottom row) aligned at the onset of sample stimulus presentation. Responses to three orientations are shown, although responses to nine orientations were recorded. Bars below histograms indicate stimulus presentation duration. Insets above rasters indicate stimuli presented: dashed lines and arrows in RDS schematically represent the surface orientation and surface normal caused by binocular disparity, respectively. Numbers at the top left of rasters indicate tilt angle. FP indicates frontoparallel orientation. (**B**) Scatter plots of preferred orientations with different types of stimulus (left column) and distribution histograms of the preferred orienta-tion difference (right column). Data for dot-TP versus line-TP are shown in the top row, and those for dot-TP versus RDS are shown in the bottom row. In scatter plots, each dot represents an individual neuron.

disparity signals have been found in the parietal (*11, 12*) and temporal (*13, 14*) association cortices. However, binocular disparity is not the only cue for depth perception, because we can perceive depth even with one eye closed. Gibson (*15*) has proposed that texture gradient is an important cue for depth perception comparable to binocular disparity. This hypothesis has been supported by psychophysical (*16*) and computational (*17*) studies. However, there have been few neurophysiological data concerning the neural correlates for the perception of depth from texture gradient cues (*18*). The purpose of this study was to examine how texture gradient cues are processed to reconstruct 3D representations of visual stimuli.

We trained two male monkeys (*Macaca fuscata*) to perform a delayed-match-to-sample (Fig. 1A) of 3D surface orientation by using the stimulus sets of texture pattern without disparity (Fig. 1B) and a random-dot stereogram (RDS) independently (*19*). During task performance, we recorded single-unit activities in the caudal part of the lateral bank of intraparietal sulcus (Fig. 1C, area CIP), where we previously had found a group of neurons selective to a 3D surface orientation of a flat surface defined by binocular disparity (*11, 12, 20, 21*). We recorded 50 neurons during performance of the matching task with texture patterns (TPs) with dot elements (dot-TPs); 70% (35/50) of them showed selective response to a texture gradient of dot-TPs. Figure 2A shows the activity of a texture gradient–sensitive neuron (*22*). This neuron showed selective response to the texture gradient of dot-TP defining 0° tilt, or right-side-nearer orientation (top row). When this neuron was further tested with another set of texture patterns, TP with line elements (line-TP), it again showed selectivity to 0° tilt (middle row). As shown in this example, 81% (13/16) of the texture gradient–sensitive neurons tested with additional line-TPs responded selectively. In these neurons, orientation selectivity was highly correlated ($r = 0.925$; $P < 0.001$) between line-TP and dot-TP (Fig. 2B, top row). The difference of preferred orientation between two conditions was <45° in all these neurons. Therefore, texture gradient–sensitive neurons were not responding to the local feature of texture patterns per se but were specifically responding to the gradient signals extracted from the texture patterns. The representative neuron also responded to RDSs and again showed selectivity to the disparity gradient defining 0° tilt (Fig. 2A, bottom row). Similar to this neuron, 77% (27/35) of texture gradient–sensitive neurons showed selectivity to a 3D surface orientation defined by disparity gradients of RDS. In these neurons, orientation selectivity was significantly correlated ($r = 0.566$; $P < 0.001$) between dot-TP and RDS (Fig. 2B, bottom row). Distribution of the difference of preferred orientation between two conditions was highly concentrated to <45° (chi-square test; $P < 0.001$). These neurons may integrate texture and disparity gradient signals to construct a generalized representation of a 3D surface orientation.

The graphs in Fig. 3 show the average responses of neurons selective to the surface orientation of dot-TP, line-TP, and RDS. For each type of stimulus set, the Gaussian curve could be fitted to average responses to eight orientations with high regression coefficients. To compare the tuning sharpness for each stimulus set, the angular deviation *S*, which corresponds to the standard deviation in the normal distribution, was calculated and averaged over neurons. The mean *S* values of all dot-TP-, line-TP-, and RDS-selective neurons were 71.3, 70.0, and 69.3, respectively, and those of 11 neurons that were selective to all types of stimuli were 68.7, 69.4, and 73.0, respectively. The averaged *S* values did not differ significantly among different types of stimuli in either case (Student's *t* test; $P > 0.10$). Thus, the neural coding of surface orientation based on texture gradient was as precise as that based on disparity gradient in CIP neurons.

After the unit recording, we conducted a behavioral test to confirm that monkeys perceive depth from texture gradient. Although psychophysical studies suggest that humans perceive depth from texture gradient (*15–17*), there are few data to suggest that animals, including monkeys, perceive depth from texture gradient as humans do. This behavioral control is important, because texture gradient is a somewhat more ambiguous cue for depth than binocular disparity. Texture per se cannot be a cue for depth; it can be a cue for depth only after its gradients have been detected. We trained monkeys to cross-match the surface orientations defined by texture and disparity gradients by using TPs without any disparity as sample stimuli and RDSs as test stimuli (*19*). Figure 4 shows the success rate in the learning and test sessions of the cross-matching of two monkeys. In the learning sessions, the performance improved gradually and reached a >80% success rate after extensive training. In the test sessions, the monkeys performed the task with a success rate significantly higher than the chance level even in the first block and showed immediate progress of performance up to a >80% success rate in the following blocks.

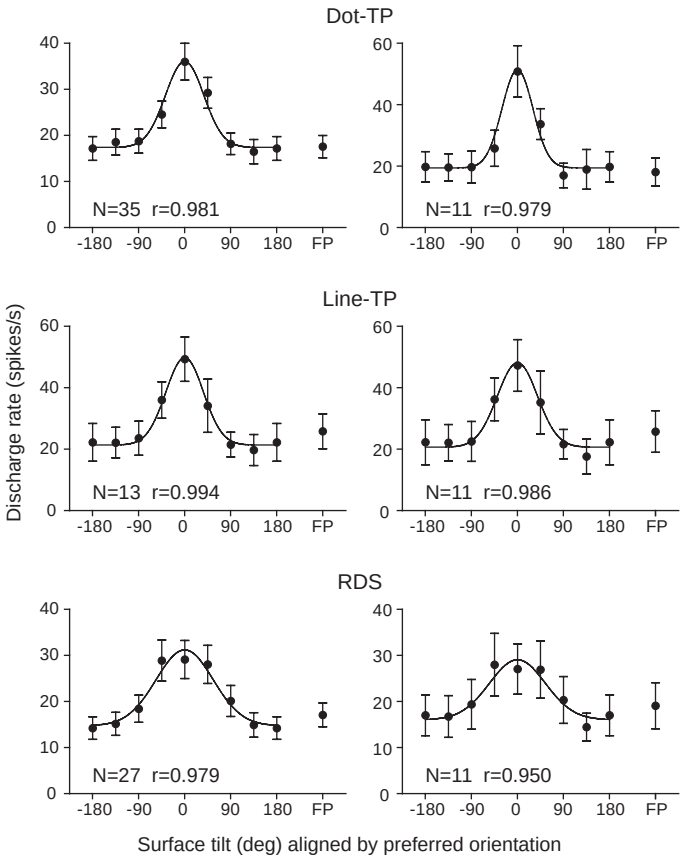

Fig. 3. Average responses to nine orientations of neurons selective to the surface orientation of dot-TP (**top**), line-TP (middle), and RDS (**bottom**). Data averaged across all neurons available for a given stimulus type are shown in the left column, and those averaged across 11 neurons that displayed surface orientation selectivity in all three stimulus types are shown in the right column. In calculating the average response, we averaged the activity of each neuron with orientation of the strongest response realigned as 0° tilt separately for each stimulus type. FP on the abscissa indicates frontoparallel orientation. Error bars indicate SE. Gaussian curve was fitted to the graphs with high regression coefficients ($r > 0.95$ and goodness of fit $P > 0.99$ for every graph).

[1]Department of Physiology and [3]Department of Neurology, Nihon University School of Medicine, Tokyo 173-8610, Japan. [2]Laboratory for Anatomy and Physiology, Seitoku Junior College of Nutrition, Tokyo 124-8530, Japan.

*Present address: Department of Anatomy, University of Cambridge, Cambridge CB2 3DY, UK.

†To whom correspondence should be addressed. E-mail: masato@med.nihon-u.ac.jp

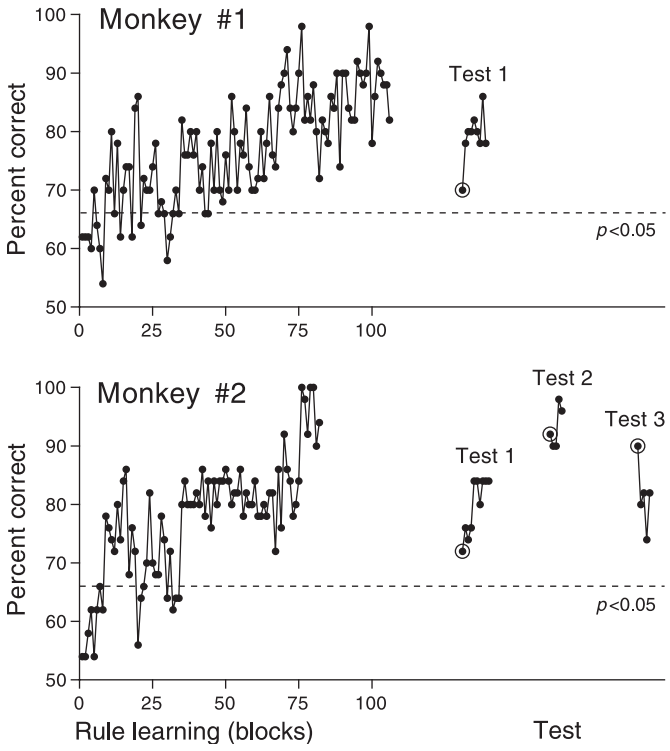

Fig. 4. Learning curve for cross-matching of TP and RDS by two monkeys. Each dot represents success rate in a block of 50 trials. Dotted lines indicate the limit of success rates above the chance level (chi-square test; $P < 0.05$) for one block. Concentric circles indicate the first block of each test session. In these test sessions, success and error trials were all reinforced to examine monkeys' performance in the absence of correct/error feedback. Note that after the learning session, the monkeys could perform the task with a success rate above the chance level even in the first block of each test session. Monkey 2 performed better in the test session with diagonal orientations (test 2) than in those with oblique orientations (tests 1 and 3), suggesting that the transfer of learning depended more on surface orientation than on texture pattern.

After learning the task rule, the monkeys could thus correctly perform the cross-matching of texture and disparity gradients even with novel orientations (tests 1 and 3) and patterns (tests 2 and 3) without training. Monkeys regarded texture and disparity gradients as equivalent depth cues, and they perceived a 3D surface orientation from texture gradient cues.

We found that texture gradient is an important cue for perceiving a 3D surface orientation for monkeys as well as humans and that neurons in CIP play a critical role in perceiving a 3D surface orientation from texture gradient. This may be the first single-unit level demonstration of the neural basis of the 3D visual perception based on texture gradient, as suggested by Gibson (*15*). As a neural correlate of 3D vision based on monocular pictorial cues, we have already found that some surface orientation–selective neurons in CIP show sensitivity to linear perspective (*12*). However, this sensitivity was relatively weak, which may be due to the ambiguity of the linear perspective cues used in the experiment. We also found in this study that most texture gradient–sensitive neurons in CIP were sensitive to disparity gradient (*23*) and that the preferences of each neuron for texture and disparity gradients were almost the same in terms of surface tilt, suggesting that they integrate texture and disparity gradient signals to construct a generalized representation of 3D surface orientation. Thus, we assume that CIP is part of the cortical circuit that is specialized for 3D vision. Recent functional imaging studies of monkeys and humans support this notion. In monkeys, LOP, a region corresponding to CIP, was activated during the presentation of 3D shapes defined by texture gradient as well as motion parallax (*24*). In humans, the caudal intraparietal area, a human homolog of CIP, was activated when subjects attended to a 3D visual feature defined by texture gradients (*25*) and other kinds of depth cues (*26, 27*). However, it is uncertain how texture gradient signals are processed before they reach CIP. As for binocular disparity signals, neurons sensitive to absolute binocular disparity have been found in the monkey striate (*4–7*) and extrastriate (*6–10*) cortices. Particularly in V3, neurons were found to be in a columnar organization based on absolute binocular disparity (*9*). Because an anatomical study suggested that CIP receives fiber projections from V3 and V3A (*28*), CIP may depend on these areas for input of binocular disparity information.

References and Notes

1. K. N. Ogle, *Binocular Vision* (Hanfer, New York, 1964).
2. B. Julesz, *Foundation of Cyclopean Perception* (Univ. of Chicago Press, Chicago, 1971).
3. I. P. Howard, B. J. Rogers, *Binocular Vision and Stereopsis* (Oxford Univ. Press, New York, 1995).
4. H. B. Barlow, C. Blakemore, J. D. Pettigrew, *J. Physiol. (London)* **193**, 327 (1967).
5. T. Nikara, P. O. Bishop, J. D. Pettigrew, *Exp. Brain Res.* **6**, 353 (1968).
6. G. F. Poggio, B. C. Motter, S. Squatrito, Y. Trotter, *Vision Res.* **25**, 397 (1985).
7. G. F. Poggio, F. Gonzalez, F. Krause, *J. Neurosci.* **8**, 4531 (1988).
8. D. H. Hubel, M. S. Livingstone, *J. Neurosci.* **7**, 3378 (1987).
9. D. L. Adams, S. Zeki, *J. Neurophysiol.* **86**, 2195 (2001).
10. D. A. Hinkle, C. E. Connor, *Nature Neurosci.* **5**, 665 (2002).
11. M. Taira, K. I. Tsutsui, M. Jiang, K. Yara, H. Sakata, *J. Neurophysiol.* **83**, 3140 (2000).
12. K. I. Tsutsui, M. Jiang, K. Yara, H. Sakata, M. Taira, *J. Neurophysiol.* **86**, 2856 (2001).
13. T. Uka, H. Tanaka, K. Yoshiyama, M. Kato, I. Fujita, *J. Neurophysiol.* **84**, 120 (2000).
14. P. Janssen, R. Vogels, G. A. Orban, *Neuron* **27**, 385 (2000).
15. J. J. Gibson, *Perception of the Visual World* (Houghton Mifflin, Boston, 1950).
16. J. E. Cutting, R. T. Millard, *J. Exp. Psychol. Genet.* **113**, 198 (1984).
17. K. A. Stevens, *Biol. Cybern.* **42**, 95 (1981).
18. Gallant *et al.* (*29*) reported that several V4 neurons responded selectively to texture gradients. However, their involvement in depth perception appeared unlikely because the activity was more influenced by 2D retinal orientation than by 3D orientation.
19. Materials and methods are available as supporting material on *Science* Online.
20. E. Shikata, Y. Tanaka, H. Nakamura, M. Taira, H. Sakata, *Neuroreport* **7**, 2389 (1996).
21. In a previous study in CIP (*12*), we found some neurons to be sensitive to a monocular cue of linear perspective in addition to binocular disparity, although its effect was weaker than the effect of binocular disparity.
22. Activities of another example of texture gradient–selective neurons are shown in fig. S1.
23. It is possible that a high proportion of texture gradient–sensitive neurons were due to training of texture gradient discrimination before unit recording. However, we consider that the existence of texture gradient–sensitive neurons is not entirely a training effect and that those neurons normally exist in CIP. In a previous study by our group (*20*), in which no discrimination was required, many CIP neurons showed selectivity to a 3D surface orientation.
24. M. E. Sereno, T. Trinath, M. Augath, N. K. Logothetis, *Neuron* **33**, 635 (2002).
25. E. Shikata *et al.*, *J. Neurophysiol.* **85**, 1309 (2001).
26. M. Taira, I. Nose, K. Inoue, K. Tsutsui, *Neuroimage* **14**, 959 (2001).
27. B. Gulyas, P. E. Roland, *Proc. Natl. Acad. Sci. U.S.A.* **91**, 1239 (1994).
28. D. L. Adams, thesis, University College London (1997).
29. J. L. Gallant, D. C. van Esssen, H. C. Nothdurft, in *Early Vision and Beyond*, T. V. Papathomas, C. Chubb, A. Gorea, E. Kowler, Eds. (MIT Press, Cambridge, MA, 1995), pp. 89–98.

30. We thank Solidray Co. for assistance in developing computer programs for 3D graphics presentation. Supported by special coordination funds for promoting science and technology, a grant to promote multidisciplinary research projects, a grant-in-aid for scientific research on priority areas ("Advanced Brain Science Project" 14017085), a grant-in-aid for scientific research (13680903), and a grant-in-aid for JSPS Fellows (199900008) from the Ministry of Education, Culture, Sports, Science and Technology, Japanese Government.

Supporting Online Material

www.sciencemag.org/cgi/content/full/298/5592/409/DC1
Materials and Methods
Fig. S1

20 May 2002; accepted 30 July 2002